Comparison of band structure and superconductivity in $FeSe_{0.5}Te_{0.5}$ and FeS*

Yang Yang(杨阳)[1], Shi-Quan Feng(冯世全)[1], Yuan-Yuan Xiang(向圆圆)[2], Hong-Yan Lu(路洪艳)[3], and Wan-Sheng Wang(王万胜)[4,†]

[1] College of Physics and Electronic Engineering, Zhengzhou University of Light Industry, Zhengzhou 450002, China
[2] College of Science, Hohai University, Nanjing 210098, China
[3] School of Physics and Electronic Information, Huaibei Normal University, Huaibei 235000, China
[4] Department of Physics, Ningbo University, Ningbo 315211, China

(Received 14 June 2017; revised manuscript received 13 July 2017; published online 20 October 2017)

The isovalent iron chalcogenides, $FeSe_{0.5}Te_{0.5}$ and FeS, share similar lattice structures but behave very differently in superconducting properties. We study the underlying mechanism theoretically. By first principle calculations and tight-binding fitting, we find the spectral weight of the $d_{X^2-Y^2}$ orbital changes remarkably in these compounds. While there are both electron and hole pockets in $FeSe_{0.5}Te_{0.5}$ and FeS, a small hole pocket with a mainly $d_{X^2-Y^2}$ character is absent in FeS. We find the spectral weights of $d_{X^2-Y^2}$ orbital change remarkably, which contribute to electron and hole pockets in $FeSe_{0.5}Te_{0.5}$ but only to electron pockets in FeS. We then perform random-phase-approximation and unbiased singular-mode functional renormalization group calculations to investigate possible superconducting instabilities that may be triggered by electron-electron interactions on top of such bare band structures. For $FeSe_{0.5}Te_{0.5}$, we find a fully gapped $s^{\pm}$-wave pairing that can be associated with spin fluctuations connecting electron and hole pockets. For FeS, however, a nodal d_{xy} (or $d_{x^2-y^2}$ in an unfolded Broullin zone) is favorable and can be related to spin fluctuations connecting the electron pockets around the corner of the Brillouin zone. Apart from the difference in chacogenide elements, we propose the main source of the difference is from the $d_{X^2-Y^2}$ orbital, which tunes the Fermi surface nesting vector and then influences the dominant pairing symmetry.

Keywords: iron-based superconductors, theories and models of superconducting state, pairing symmetry

PACS: 74.20.–z, 74.20.Pq, 74.20.Rp **DOI:** 10.1088/1674-1056/26/12/127401

1. Introduction

The discovery of superconductivity in fluorine doped LaFeAsO has stimulated tremendous research efforts in iron-based superconductors (FeSCs) in recent years.[1] Different families of FeSCs have been detected since then. Among them, the 11 family iron–chalcogen (Fe*Ch*) with *Ch* = S, Se, Te have been extensively studied due to them having the simplest crystal structure but intriguing superconducting properties. A central issue in studying 11 family Fe*Ch* is to determine the pairing symmetry and gap structure. For example, in FeSe, the gap structure is still under debate. The presence of gap nodes is observed by scanning tunneling spectroscopic (STS) measurements,[2,3] while some experiments such as specific heat and thermal conductivity suggest nodeless gaps.[4,5] With Te substitution, for optimally doped $FeSe_{0.5}Te_{0.5}$, the superconducting gap is believed to be isotropically full-gapped.[6–8] For FeS (Ref. [9]), the recent low-temperature heat transport measurements have revealed a nodal quasiparticle behavior.[10,11] Furthermore, theoretical calculation suggests that the paring symmetry is a $d_{x^2-y^2}$ wave.[12] Although the 11 family Fe*Ch* share the same crystal structure and similar electronic structure, the gap structure seems to be different. Therefore, it is interesting to discuss the similarity and difference within 11 family Fe*Ch*.

To elucidate the mechanism behind the evolution of the paring symmetry, one clue is the effect of the lattice structure on the electronic structure near the Fermi energy, which may change the spin fluctuation.[13] However, this interplay picture has not yet been clarified in FeSCs. The 11 family Fe*Ch* may offer a good platform to study the mechanism behind the pairing symmetry transition owing to their very simple crystal structures. In this regard, a comparison among different members of this family is necessary.

In this work, we mainly compare the electronic structures and microscopic pairing mechanism between FeS and $FeSe_{0.5}Te_{0.5}$. FeS exhibits nodal behavior, while $FeSe_{0.5}Te_{0.5}$ is believed to be a nodeless full-gapped superconductor clarified by experiments. We present the electronic calculation based on density functional theory (DFT) and construct a theoretical model using a maximally-localized Wannier functions (MLWFs) method. The microscopic interplay between spin fluctuation and superconductivity is studied using both random-phase-approximation (RPA) and singular-mode functional renormalization group (SMFRG) methods.

*Project supported by the National Natural Science Foundation of China (Grant Nos.11604303, 11604168, and 11574108).
†Corresponding author. E-mail: 2014070@zzuli.edu.cn
© 2017 Chinese Physical Society and IOP Publishing Ltd

Our main findings are listed as follows. We find that for $FeSe_{0.5}Te_{0.5}$ and FeS, the electronic structures are similar except some small difference in projected density of states (pDOS) and Fermi surfaces. With Ch height changing, the Fe $d_{X^2-Y^2}$ orbital components on Fermi surfaces change remarkably, which contributes to electron and hole pockets in $FeSe_{0.5}Te_{0.5}$ but only to hole pockets in FeS. The SMFRG results show that for $FeSe_{0.5}Te_{0.5}$, a full-gapped $s\pm$-wave pairing is triggered by spin fluctuations connecting electron and hole pockets. Whereas for FeS, a nodal d_{xy}-wave pairing is induced by small spin wave vectors. The form factors of pairing functions show that intraorbital scattering of $d_{X^2-Y^2}$ plays an important role in pairing of FeS, related with the changes of orbital components. Therefore, we propose the different crystal structures and *Ch* atoms will bring two tendencies: the enhanced intraorbital scattering and the change of orbital components on Fermi surfaces, especially for the $d_{X^2-Y^2}$ orbital, which facilitate the pairing symmetry from a full-gapped $s\pm$-wave evolved into a nodal d-wave.

2. DFT calculations

Since the details of DFT calculations about FeS have been reported in our former work,[12] we focus on $FeSe_{0.5}Te_{0.5}$ now. For $FeSe_{0.5}Te_{0.5}$ composition, the unit cell in the tetragonal phase of the PbO-type is used in our following studies, shown in Fig. 1. This arrangement requires only a replacement of one Se by the Te atom in the single unit cell of FeSe. Furthermore, different arrangements of Te are tested within the $2 \times 2 \times 1$ supercell by DFT calculation, and the total energies are very similar. So we choose this convenient atomic configuration, following the same way as former DFT studies.[14–16]

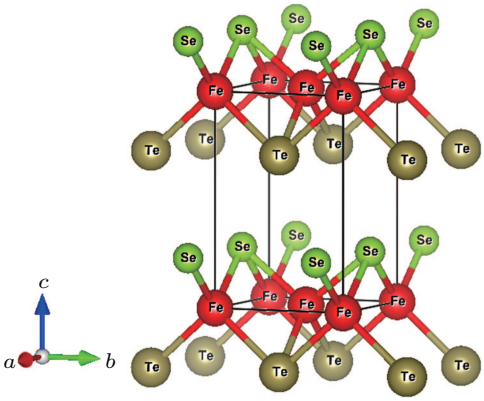


Fig. 1. (color online) The unit cell of $FeSe_{0.5}Te_{0.5}$ with the alternate arrangement of Se and Te atoms.

The crystallographic parameters are taken from neutron diffraction data in Ref. [14]. The Se and Te ions occupy different atomic sites, which leads to two inter-cell positions, z_{Se} and z_{Te}. For experimental values $z_{Se} = 0.244$ and $z_{Te} = 0.285$. Compared with FeS, the Ch heights are enlarged from 1.269 Å to 1.453/1.697 Å owing to the bigger ionic radius of selenium and tellurium atoms. We use the preliminary experimental values and then relax the height of the chalcogen. The fractional coordinates $z_{Se} = 0.220$ and $z_{Te} = 0.270$ are determined after relaxation. We perform our calculation for both of the experimental values and optimized values, the results are almost the same and we mainly discuss the results for experimental values below.

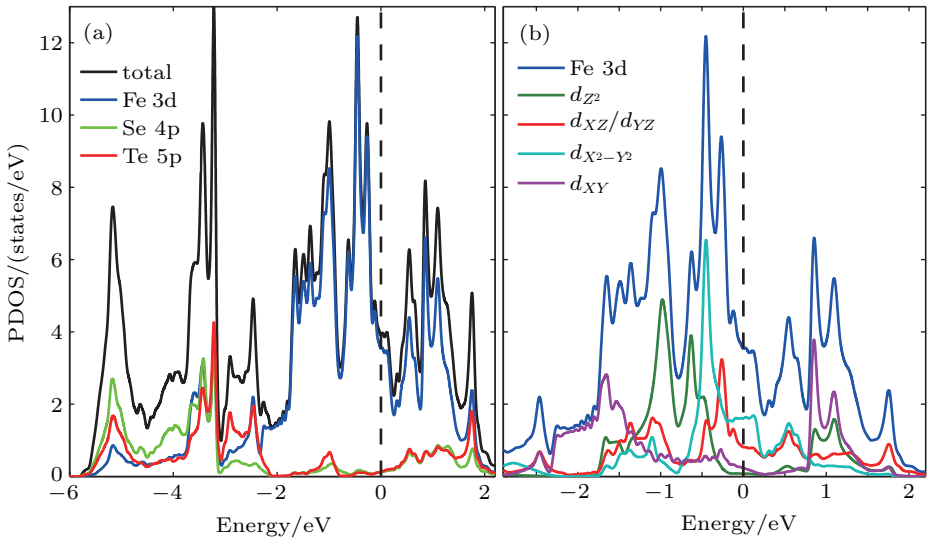


Fig. 2. (color online) (a) Total DOS and pDOS obtained by DFT. (b) The pDOS from all five orbitals of Fe 3d, the X, Y, Z refer to axes for a unit cell with two Fe atoms.

Electronic structure calculations for $FeSe_{0.5}Te_{0.5}$ have been performed via the Quantum ESPRESSO code in the framework of DFT.[17] The PAW pseupotentials are adopted and the exchange correlation is considered by the generalized gradient approximation (GGA) of Perdew–Burke–Ernzerhof.[18] After the total energy convergence test, we choose 62-Ry (1 Ry = 13.6056923 eV) energy cut off to ensure accuracy. Self-consistent calculations were converged on

a $12 \times 12 \times 12$ k-point grid and $36 \times 36 \times 36$ k-point grid was used for non-consistent calculations.

The density of states are shown in Fig. 2. It is obvious that the DOS are divided into two parts. The Se 3p and Te 4p states concentrate from -6.0 eV to -2.5 eV below Fermi energy E_F. The Fe 3d states dominate from -2.5 eV to 2.5 eV around E_F. The pDOS onto five Fe 3d orbitals are shown in Fig. 2(b). At E_F, one finds that the d_{XZ}/d_{YZ} and $d_{X^2-Y^2}$ (the X, Y, Z refer to axes for unit cell with two Fe atoms) provide the main contributions. Compared with FeS, the value of $N(E_F) = 3.91$ eV^{-1} is larger than that of FeS, which has a value of $N(E_F) = 2.30$ eV^{-1}. The pDOS of $d_{X^2-Y^2}$ contributes a lot to this difference, which becomes bigger in $FeSe_{0.5}Te_{0.5}$ than FeS. The other trend noted is that the pseudogap of DOS near $N(E_F)$ is rather smaller than FeS. It is ascribed to the evolution of the Ch height. When the Ch height decreases, the interorbital hoppings are enhanced, thus leading to the splitting of the Fe 3d bands into lower and upper bands.[19]

Figure 3 shows the band structure of $FeSe_{0.5}Te_{0.5}$. There are five bands across E_F, forming five disconnected Fermi surface sheets, as shown in Fig. 4. Two cylinders are around the M–A line to construct two rather similar electron pockets. Three hole cylinders including an innermost closed pocket are around the Γ–Z line. The results share great similarities with a former angle-resolved photoemission spectroscopy (ARPES) study of $Fe_{1.04}(Te_{0.66}Se_{0.34})$.[20] Moreover, for an optimized Ch height, it gives qualitatively similar band structures and Fermi surface around E_F, except the innermost hole pocket gets bigger. For FeS, the innermost hole pocket is absent and both the electron and hole pockets are reduced. The band filling is reduced from 12.00 for $FeSe_{0.5}Te_{0.5}$ to 11.92 for FeS.

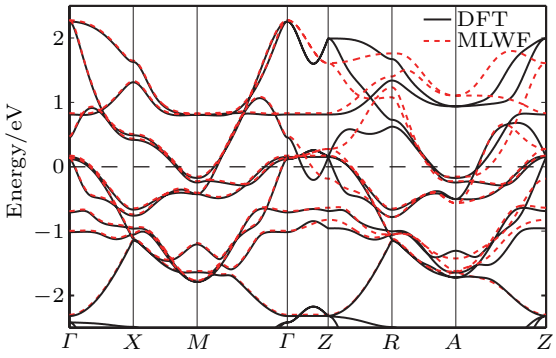


Fig. 3. (color online) Band structure of $FeSe_{0.5}Te_{0.5}$ obtained by DFT calculations (solid black lines) and MLWF fitting (dashed red lines).

The band structures are then fitted by means of the MLWF method.[21,22] There are ten Wannier functions centered at two Fe sites in the unit cell. As shown in Fig. 3, the MLWFs fit the band structure rather accurately in the $k_z = 0$ plane. It is noted that unlike the case of FeSe or FeS, the local arrangement of each Fe atom in the unit cell is different due to the different surroundings of Se and Te atom. Therefore, we cannot further unfold the Brillouin zone with one Fe atom per unit cell, and thus we only consider the ten-orbital theoretical model.

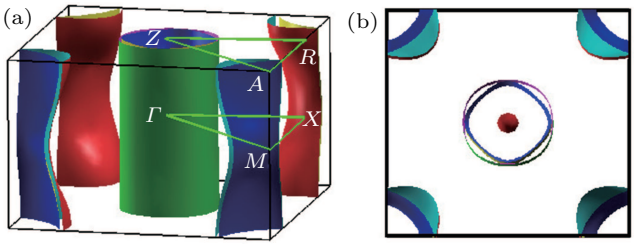


Fig. 4. (color online) Lateral view (a) and top view (b) of Fermi surface sheets for $FeSe_{0.5}Te_{0.5}$.

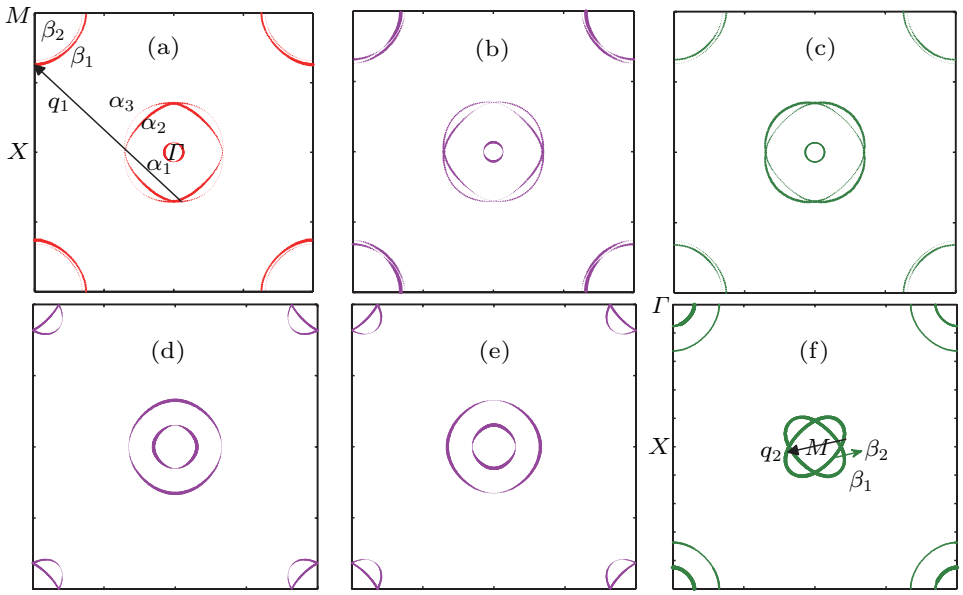


Fig. 5. (color online) Fermi surface sheets of $FeSe_{0.5}Te_{0.5}$ (top) and FeS (bottom) in the 2Fe unit cell. The width of each Fermi surfaces line is proportional to its spectral weights in d_{XZ}, d_{YZ}, and $d_{X^2-Y^2}$ components, respectively. The hole pockets around Γ are denoted by α_1, α_2, and α_3 from the inside out. The electron pockets are denoted by β_1 and β_2, respectively. The α_1 is absent for FeS. The arrows in panels (a) and (f) denote the possible dominant scattering vectors $\boldsymbol{q}_1$ for $FeSe_{0.5}Te_{0.5}$ and $\boldsymbol{q}_2$ for FeS, respectively.

3. Correlation effects

It has been suggested that the orbital character plays an important role in determining the pairing symmetry for FeSCs. To address this issue, the Fermi surface of $FeSe_{0.5}Te_{0.5}$ and FeS encoded with the spectral weights in d_{XZ}, d_{YZ}, and $d_{X^2-Y^2}$ orbital components are obtained and shown in Figs. 5(a)–5(f). Specifically, for $FeSe_{0.5}Te_{0.5}$, the d_{XZ}/d_{YZ} contribute mainly to the α_1, α_2 pocket and β_1, β_2 pockets. Whereas the $d_{X^2-Y^2}$ (refers to d_{xy} in an unfolded Brillouin zone) contribute mainly to the α_3 pocket and some spectral weights to the β_1, β_2 pockets. For FeS, the orbital composition changes substantially. One major difference is the α_2, α_3 hole pockets around Γ have the few $d_{X^2-Y^2}$ character, instead the β_1, β_2 electron pockets around M have mainly the $d_{X^2-Y^2}$ character. Seen from the Fermi surface in Fig. 5(a)–5(f), there are some different types of spin fluctuation, including the interpocket scattering between hole and electron pockets labeled as $\boldsymbol{q}_1$ and scattering between electron pockets labeled as $\boldsymbol{q}_2$. Intuitively, the leading scattering will be changed due to the change of $d_{X^2-Y^2}$ orbital components. To check this, we should consider the correlation effects.

We consider the following local interactions as,

$$\begin{aligned} H_{\mathrm{I}} = & U\sum_{i\mu} n_{i\mu\uparrow}n_{i\mu\downarrow} + U'\sum_{i,\mu>\nu} n_{i,\mu}n_{i,\nu} \\ & + J_{\mathrm{H}}\sum_{i,\mu>\nu,\sigma\sigma'} c^{\dagger}_{i\mu\sigma}c_{i\nu\sigma}c^{\dagger}_{i\nu\sigma'}c_{i\mu\sigma'} \\ & + J_{\mathrm{H}}\sum_{i,\mu\neq\nu} c^{\dagger}_{i\mu\uparrow}c^{\dagger}_{i\mu\downarrow}c_{i\nu\downarrow}c_{i\nu\uparrow}, \end{aligned} \tag{1}$$

where i denotes lattice sites, σ is the spin polarity, μ and ν denote ten Fe 3d orbitals, $n_{i\mu} = \sum_{\sigma} c^{\dagger}_{i\mu\sigma}c_{i\mu\sigma}$, U is the on-site intra-orbital repulsion, J_{H} is Hund's rule coupling, and we use the Kanamori relation $U' = U - 2J_{\mathrm{H}}$.

We first calculate the bare susceptibilities and random-phase-approximation (RPA) spin susceptibilities for both systems based on the theoretical models discussed above. The main results are summarized in Fig. 6. The bare susceptibilities for both systems share great similarities with each other, owing to the similar Fermi surface topology. They both have dominant peaks at the zone corner and some broad peaks around the zone center. However, as the interaction is introduced, the spin fluctuations of these two systems diverge obviously. For $FeSe_{0.5}Te_{0.5}$, the predominant peaks around (π,π) are enhanced rapidly. While for FeS, the peaks around the zone center become stronger, reflecting that the spin fluctuation is different from $FeSe_{0.5}Te_{0.5}$. We also check pairing interactions due to spin fluctuations from the RPA framework. For both $FeSe_{0.5}Te_{0.5}$ and FeS, we see different pairing channels compete with the value of U changes, the same as former RPA studies for other FeSCs.[13,23,24] Thus, we should consider the competing collective fluctuation in density-wave and pairing channels in these systems, which we resort to the unbiased SMFRG developed recently. Meanwhile, it has an advantage in getting more reliable pairing functions in orbital basis, from which we can obtain the main difference of the pairing mechanism between $FeSe_{0.5}Te_{0.5}$ and FeS.

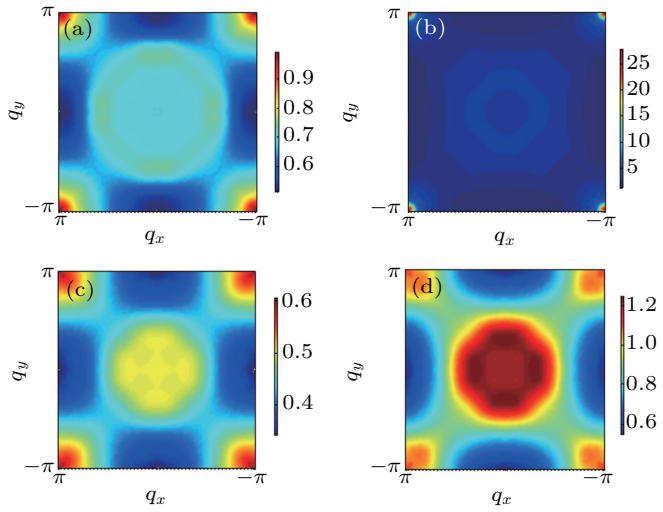


Fig. 6. (color online) Left panels: The bare suceptibilities for $FeSe_{0.5}Te_{0.5}$ (a) and FeS (c), respectively. Right panels: The RPA spin suceptibilities for $FeSe_{0.5}Te_{0.5}$ (b) and FeS (d), respectively. Here, $U = 0.9$ eV and $J_{\mathrm{H}} = U/5$.

Starting from the bare interactions in H_{I}, SMFRG provides the flow versus a decreasing infrared energy cutoff Λ of the effective one-particle-irreducible four-point interaction vertex function. In a nutshell, the latter can also be understood as a generalized pseudo-potential running with Λ. The divergence of the vertex function versus decreasing Λ signals an instability of the normal state. To see the instability channel, from the vertex function we extract the scattering matrices between fermion bilinears in the general charge-density-wave (CDW), SDW and SC channels. For a given channel, and for a given collective momentum $\boldsymbol{q}$,[26] the scattering matrix can be decomposed into eigen modes as

$$V^{\alpha\beta;\gamma\delta}(\boldsymbol{k},\boldsymbol{k}',\boldsymbol{q}) \to \sum_{m} \phi_m^{\alpha\beta}(\boldsymbol{k}) S_m [\phi_m^{\gamma\delta}(\boldsymbol{k}')]^*, \tag{2}$$

where S_m is the eigenvalue and $\phi_m(\boldsymbol{k})$ is a form factor (a function of internal momentum $\boldsymbol{k}$ and a matrix in the orbital basis). During the FRG flow, we monitor the leading attractive eigen mode in each channel (and at each collective momentum). The most attractive and diverging one in all channels decides the global instability, implying an emerging order described by the associated collective momentum $\boldsymbol{Q}$ and the matrix form factor $\phi(\boldsymbol{k})$. More details can be found elsewhere.[25–33]

We first discuss the results for $FeSe_{0.5}Te_{0.5}$. Figure 7(a) shows the FRG flow versus Λ (the infrared cutoff of the Matsubara frequency) for $U = 1.40$ eV and $J_{\mathrm{H}} = U/5$. Since the CDW channel remains weak during the flow, we shall not discuss it henceforth. We find the interaction in the SDW channel is enhanced in the intermediate stage but levels off at low-energy scales. The associated collective momentum $\boldsymbol{Q}$ evolves

(as indicted by the arrows) from $\boldsymbol{Q} = (0,0)$ and eventually settles down at $\boldsymbol{Q} = (0.95, 0.98)\pi$. The small hump in the flow of $S_{\rm SDW}$ suggests the leading spin fluctuation undergoes a change. The inset shows $S_{\rm SDW}(\boldsymbol{q})$ versus $\boldsymbol{q}$ at the final stage. There are predominant peaks around (π, π), corresponding to $\boldsymbol{q}_1$ scattering between the hole pockets and electron pockets in Fig. 5(a). As spin fluctuations are enhanced, the attractive pairing interaction $S_{\rm SC}$ is enhanced significantly and eventually diverges. The details of the pairing form factors for $S_{\rm SC}$ can be found in Appendix A. The form factor $\phi_{\rm SC}$ turns out to be dominated by the nearest bond from mainly (d_{XZ}, d_{YZ}) orbitals, which is closely related with the orbital components discussed above. The pairing symmetry is dictated by the leading form factor. To see this straightforwardly, we further project the form factor into the band basis and plot it along the Fermi surfaces in Fig. 7(b). Obviously, the gap is isotropic on each pocket and describes a full-gapped $s\pm$-wave, consistent with former experiments.[6–8]

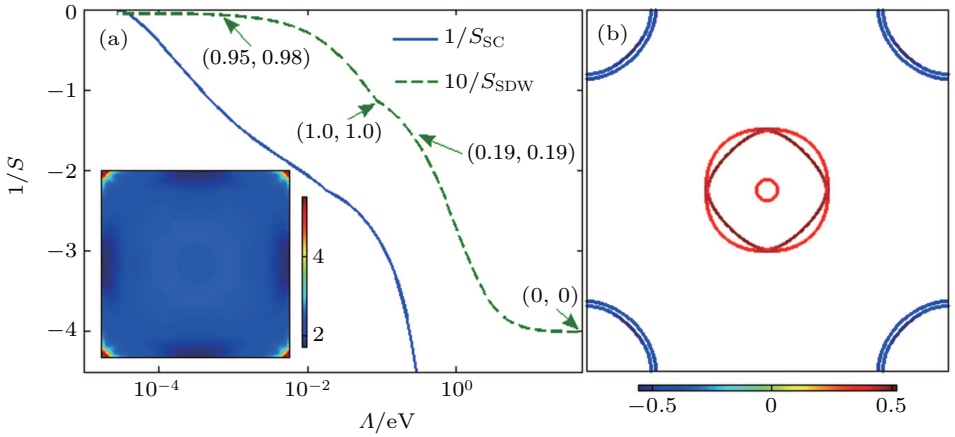


Fig. 7. (color online) (a) FRG flow of $1/S_{\rm SC,SDW}$ versus Λ for $U = 1.4$ eV and $J_{\rm H} = U/5$ for $FeSe_{0.5}Te_{0.5}$. The arrows indicate snapshots of the leading momentum $\boldsymbol{Q}$ (divided by π) in the SDW channel. The inset shows $|S_{\rm SDW}(\boldsymbol{q})|$ in the momentum space at the final energy scale. (b) The gap funtion $\Delta(\boldsymbol{k})$ on the k points of Fermi surfaces for $FeSe_{0.5}Te_{0.5}$.

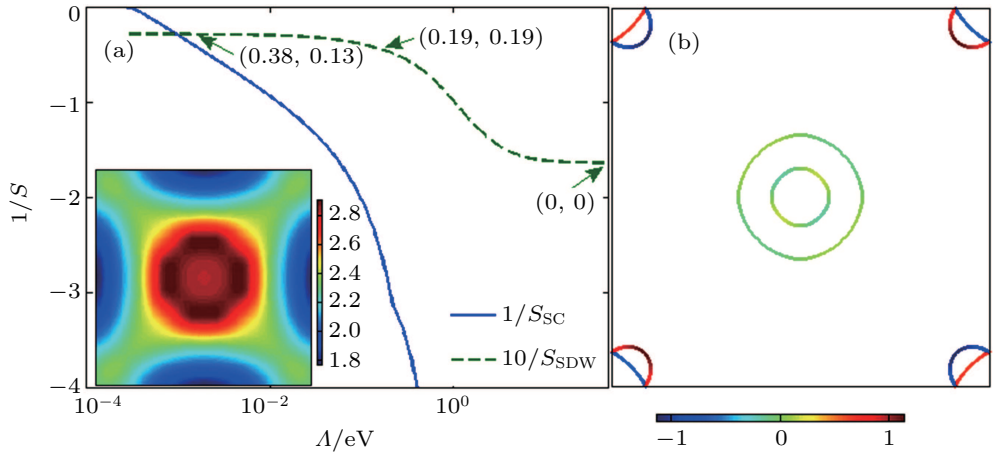


Fig. 8. (color online) (a) FRG flow of $1/S_{\rm SC,SDW}$ versus Λ for $U = 1.7$ eV and $J_{\rm H} = U/5$ for FeS. The arrows indicate snapshots of the leading momentum $\boldsymbol{Q}$ (divided by π) in the SDW channel. The inset shows $|S_{\rm SDW}(\boldsymbol{q})|$ in the momentum space at the final energy scale. (b) The gap function $\Delta(\boldsymbol{k})$ on the k points of Fermi surfaces for FeS.

We now discuss the case for FeS. For comparison, a ten-orbital model with two Fe atoms is used. The FRG flow for $U = 1.70$ eV and $J_{\rm H} = U/5$ is shown in Fig. 8(a). The interaction in the SDW channel, $S_{\rm SDW}$ behaves qualitatively similar to $FeSe_{0.5}Te_{0.5}$ at the beginning but does not undergo transition to (π, π) at intermediate stages. Eventually, $S_{\rm SDW}$ levels off at low-energy scales, associated with small collective momentum $\boldsymbol{Q} = (0.38, 0.13)\pi$. The inset of Fig. (a) shows $S_{\rm SDW}(\boldsymbol{q})$ versus $\boldsymbol{q}$ at the final stage of the flow. Incommensurate peaks around the zone center are obvious. According to the orbital components in Figs. 5(d)–5(f), this small momentum corresponds mainly to the interpocket scattering between β_1 and β_2, which is labeled by $\boldsymbol{q}_2$ in Fig. 5(f). The reason consists in two aspects. First, the interorbital hoppings are enhanced due to the reduction of Ch height in FeS, leading to the enhanced interorbital scattering. Second, α_1, α_2 pockets have few $d_{X^2-Y^2}$ components whereas the β_1 and β_2 have mainly $d_{X^2-Y^2}$ components. Therefore, the small momentum can benefit from different types of scattering and become the leading eigenvalue. Triggered by such spin fluctuations, the pairing interaction is enhanced and eventually diverges. The pairing form factors can be seen in Appendix A for details. It de-

scribes pairing on the nearest bond. Moreover, the most active orbital for this pairing state is $d_{X^2-Y^2}$, corresponding to the interpocket scattering between β_1 and β_2. We further project the form factor into the band basis. As is shown in Fig. 8(b), the pairing symmetry transforms as d_{xy} (refer to $d_{x^2-y^2}$ in an unfolded Broullin zone) along Fermi surfaces. It is fully gapped on the β_1, β_2 pockets but nodal on the α_1, α_2 pockets, which is consistent with nodal behavior in experiments.[10,11]

Firstly, we emphasize that the pairing symmetry we obtained from FRG is consistent with our RPA results when U is big enough. Secondly, we have performed systematic calculations for other values of $(U, J_{\rm H})$. We find $FeSe_{0.5}Te_{0.5}$ is in close proximity to the antiferromagnetism phase. For $U > 1.40$, the $S_{\rm SDW}$ quickly diverges at high-energy scales and the system develops an SDW instability at large wave vectors. On the other hand, for the case of FeS, the system develops SC instability until $U \sim 2.10$. For $U > 2.10$, the system develops SDW instability at small wave vectors. Given the experimental results, the wave vectors around (π, π) connecting the Γ and M pockets has been observed in $FeSe_xTe_{1-x}$ and $BaFe_2As_2$-derived superconductors, which is seen as a common feature among most FeSCs.[34–38] For FeS, the magnetic properties are sensitive to structural details and the previously reported sample with $a > 3.68$ Å show bulk superconductors with no magnetism. The recent temperature neutron diffraction data for the $a \approx 3.674$ Å sample has real spin wave vectors $k_m = (0.25, 0.25, 0)$,[39] reflecting FeS have different magnetic ordering with $Fe_{0.5}Te_{0.5}$. Combined with our results, we propose that, for moderate U, the much stronger spin fluctuation in $FeSe_{0.5}Te_{0.5}$ will induce the superconductivity at a higher energy scale. It may explain why $FeSe_{0.5}Te_{0.5}$ ($T_{\rm c} \sim 15.2$ K) have higher superconducting transition temperature than FeS ($T_{\rm c} \sim 4.5$ K).

4. Summary and conclusions

We have compared the electronic structure and correlation effects of $FeSe_{0.5}Te_{0.5}$ with FeS. The electronic structures are similar except for some difference, the $N(E_{\rm F})$ of $FeSe_{0.5}Te_{0.5}$ is larger than FeS owing to the increase of Fe $d_{X^2-Y^2}$ orbital pDOS. An innermost hold pocket is present (absent) in $FeSe_{0.5}Te_{0.5}$ (FeS). Furthermore, for orbital components along the Fermi surfaces, we find the $d_{X^2-Y^2}$ orbital character significantly changed, which mainly contribute to an electron pocket around M in FeS. To study the interplay of the electronic structure and pairing symmetry, we have performed RPA and SMFRG calculation based on ten Fe 3d orbital models. The results shown in $FeSe_{0.5}Te_{0.5}$, a full-gap $s\pm$ is induced by wave vectors around (π, π) connecting electron and hole pockets. Whereas in FeS, a nodal d_{xy} (refer to $d_{x^2-y^2}$ in the unfolded Brillouin zone) pairing is induced by a small wave vector coming from the interpocket scattering of electron pockets. This evolution of pairing symmetry is closely related to the change of $d_{X^2-Y^2}$ orbital components on Fermi surfaces. As crystal structures change from $FeSe_{0.5}Te_{0.5}$ to FeS, the intraorbital scattering of $d_{X^2-Y^2}$ is enhanced and the $\beta_1 - \beta_2$ nesting becomes dominant. The leading form factor of the pairing function obtained by SMFRG also support this propose.

Appendix A: Form factors and gap function in the band basis

In this appendix we give the expressions of the form factors, or pairing matrix, $\phi_{\rm SC}(\boldsymbol{k})$ in the orbital basis. To describe the momentum dependence, we introduce the lattice harmonics

$$\begin{aligned} c_x &= \cos \boldsymbol{k}_x, \quad c_{x/2} = \cos(\boldsymbol{k}_x/2), \\ c_y &= \cos \boldsymbol{k}_y, \quad c_{y/2} = \cos(\boldsymbol{k}_y/2), \\ s_x &= \sin \boldsymbol{k}_x, \quad s_{x/2} = \sin(\boldsymbol{k}_x/2), \\ s_y &= \sin \boldsymbol{k}_y, \quad s_{y/2} = \sin(\boldsymbol{k}_y/2). \end{aligned} \tag{A1}$$

The leading pairing functions $\phi_{\rm SC}(\boldsymbol{k})$ of $FeSe_{0.5}Te_{0.5}$ are described in the orbital basis as for (A–A),

$$\begin{aligned} \phi_{\rm SC}^{11}(\boldsymbol{k}) &= -0.07 + 0.13(c_x + c_y) \\ \phi_{\rm SC}^{14}(\boldsymbol{k}) &= \phi_{\rm SC}^{41}(\boldsymbol{k}) = 0.13 - 0.11c_x - 0.11c_y, \\ \phi_{\rm SC}^{22}(\boldsymbol{k}) &= 0.06 + 0.16c_x + 0.09c_y, \\ \phi_{\rm SC}^{33}(\boldsymbol{k}) &= 0.28 + 0.12c_x + 0.16c_y, \\ \phi_{\rm SC}^{44}(\boldsymbol{k}) &= -0.26 + 0.11c_x + 0.10c_y, \\ \phi_{\rm SC}^{55}(\boldsymbol{k}) &= -0.24 + 0.01(c_x + c_y), \end{aligned} \tag{A2}$$

for (A–B),

$$\begin{aligned} \phi_{\rm SC}^{11}(\boldsymbol{k}) &= -0.29c_{x/2}c_{y/2}, \\ \phi_{\rm SC}^{15}(\boldsymbol{k}) &= \phi_{\rm SC}^{51}(\boldsymbol{k}) = -0.01s_{x/2}s_{y/2}, \\ \phi_{\rm SC}^{22}(\boldsymbol{k}) &= \phi_{\rm SC}^{33}(\boldsymbol{k}) = -0.36c_{x/2}c_{y/2}, \\ \phi_{\rm SC}^{23}(\boldsymbol{k}) &= -0.36s_{x/2}s_{y/2}, \\ \phi_{\rm SC}^{32}(\boldsymbol{k}) &= -0.31s_{x/2}s_{y/2}, \\ \phi_{\rm SC}^{44}(\boldsymbol{k}) &= 0.27c_{x/2}c_{y/2}, \\ \phi_{\rm SC}^{55}(\boldsymbol{k}) &= -0.14c_{x/2}c_{y/2}, \end{aligned} \tag{A3}$$

for (B-B),

$$\begin{aligned} \phi_{\rm SC}^{11}(\boldsymbol{k}) &= -0.07 + 0.13(c_x + c_y), \\ \phi_{\rm SC}^{14}(\boldsymbol{k}) &= \phi_{\rm SC}^{41}(\boldsymbol{k}) = -0.13 + 0.11c_x + 0.11c_y, \\ \phi_{\rm SC}^{22}(\boldsymbol{k}) &= 0.28 + 0.16c_x + 0.12c_y, \\ \phi_{\rm SC}^{33}(\boldsymbol{k}) &= 0.06 + 0.09c_x + 0.16c_y, \\ \phi_{\rm SC}^{44}(\boldsymbol{k}) &= -0.26 + 0.10c_x + 0.11c_y, \\ \phi_{\rm SC}^{55}(\boldsymbol{k}) &= -0.24 + 0.01(c_x + c_y). \end{aligned} \tag{A4}$$

The superscript number (1, 2, 3, 4, 5) denotes the 3d orbital (d_{Z^2}, d_{XZ}, d_{YZ}, $d_{X^2-Y^2}$, d_{XY}) for one Fe atom. (A, B) denote

two sublattices for the unit cell. The transform from $A(B)$ to $A(B)$ and $A(B)$ to $B(A)$ satisfies the C_{4v} point group symmetry. It is noted in this case the center of the point group locates at the center of the Fe-square, owing to the different surroundings. That means for 90-degree rotation, the Fe atom also needs to be changed from one to another. After checking the symmetry of the form factor, we find it describes an s-wave pairing state.

With the pairing matrix $\phi_{\rm SC}$ in the orbital basis, the gap function in the band basis is given by $\Delta_{\boldsymbol{k}n} = \langle \boldsymbol{k}n|\phi_{\rm SC}(\boldsymbol{k})|\boldsymbol{k}n\rangle$ where n is the band label and $|\boldsymbol{k}n\rangle$ is the Bloch state in the given band.

The leading pairing functions $\phi_{\rm SC}(\boldsymbol{k})$ of FeS are given by

$$\begin{aligned}
&\phi^{11}_{\rm SC}(\boldsymbol{k}) = -0.01 s_{x/2}s_{y/2},\\
&\phi^{15}_{\rm SC}(\boldsymbol{k}) = \phi^{51}_{\rm SC}(\boldsymbol{k}) = -0.02 - 0.02(c_{x/2}c_{y/2}),\\
&\phi^{22}_{\rm SC}(\boldsymbol{k}) = \phi^{33}_{\rm SC}(\boldsymbol{k}) = -0.25 s_{x/2}s_{y/2},\\
&\phi^{23}_{\rm SC}(\boldsymbol{k}) = \phi^{32}_{\rm SC}(\boldsymbol{k}) = 0.14 - 0.02(c_x + c_y) - 0.08 c_{x/2}c_{y/2},\\
&\phi^{44}_{\rm SC}(\boldsymbol{k}) = -1.30 s_{x/2}s_{y/2}. \qquad \text{(A5)}
\end{aligned}$$

In this case, the axis of rotation crosses one of the two Fe atoms in the unit cell. It is obvious that the form factors obey the C_{4v} point group symmetry. Under point group operation of orbital and momentum, the form factor transforms as d_{xy}-wave pairing.

Acknowledgment

Yang Yang thanks Qiang-Hua Wang for helpful discussions.

References

[1] Kamihara Y, Watanabe T, Hirano M and Hosono H 2008 *J. Am. Chem. Soc.* **130** 3296

[2] Song C L, Wang Y L, Cheng P, Jiang Y P, Li W, Zhang T, Li Z, He K, Wang L L, Jia J F, Huang H H, Wu C J, Ma X C, Chen X and Xue Q K 2011 *Science* **332** 1410

[3] Kasahara S, Watashige T, Hanaguri T, Kohsaka Y, Yamashita T, Shimoyama Y, Mizukami Y, Endo R, Ikeda H, Aoyama K, Terashima T, Uji S, Wolf T, L?hneysen H v, Shibauchi T and Matsuda Y 2014 *Proc. Natl. Acad. Sci. USA* **111** 16309

[4] Dong J K, Guan T Y, Zhou S Y, Qiu X, Ding L, Zhang C, Patel U, Xiao Z L and Li S Y 2009 *Phys. Rev. B* **80** 024518

[5] Lin J Y, Hsieh Y S, Chareev D A, Vasiliev A N, Parsons Y and Yang H D 2011 *Phys. Rev. B* **84** 220507

[6] Hanaguri T, Niitaka S, Kuroki K and Takagi H 2010 *Science* **328** 474

[7] Miao H, Richard P, Tanaka Y, Nakayama K, Qian T, Umezawa K, Sato T, Xu Y M, Shi Y B, Xu N, Wang X P, Zhang P, Yang H B, Xu Z J, Wen J S, Gu G D, Dai X, Hu J P, Takahashi T and Ding H 2012 *Phys. Rev. B* **85** 094506

[8] Okazaki K, Ito Y, Ota Y, Kotani Y, Shimojima T, Kiss T, Watanabe S, Chen C T, Niitaka S, Hanaguri T, Takagi H, Chainani A and Shin S 2012 *Phys. Rev. Lett.* **109** 237011

[9] Lai X, Zhang H, Wang Y, Wang X, Zhang X, Lin J and Huang F 2015 *J. Am. Chem. Soc.* **137** 10148

[10] Ying T, Lai X, Hong X, Xu Y, He L, Zhang J, Wang M, Yu Y, Huang F and Li S 2016 *Phys. Rev. B* **94** 100504

[11] Xing J, Lin H, Li Y, Li S, Zhu X, Yang H and Wen H H 2016 *Phys. Rev. B* **93** 104520

[12] Yang Y, Wang W S, Lu H Y, Xiang Y Y and Wang Q H 2016 *Phys. Rev. B* **93** 104514

[13] Kuroki K, Usui H, Onari S, Arita R and Aoki H 2009 *Phys. Rev. B* **79** 224511

[14] Louca D, Horigane K, Llobet A, Arita R, Ji S, Katayama N, Konbu S, Nakamura K, Koo T Y, Tong P and Yamada K 2010 *Phys. Rev. B* **81** 134524

[15] Ciechan A, Winiarski M J and Czekala M S 2012 *Acta Physica Polonica A* **121** 820

[16] Ciechan A, Winiarski M J and Czekala M S 2013 *Intermetallics* **41** 44

[17] Giannozzi P, *et al.* 2009 *J. Phys.: Condens. Matter* **21** 395502

[18] Perdew J P, Burke K and Ernzerhof M 1996 *Phys. Rev. Lett.* **77** 3865

[19] Miyake T, Nakamura K, Arita R and Imada M 2010 *J. Phys. Soc. Jpn.* **79** 044705

[20] Chen F, Zhou B, Zhang Y, Wei J, Ou H W, Zhao J F, He C, Ge Q Q, Arita M, Shimada K, Namatame H, Taniguchi M, Lu Z Y, Hu J, Cui X Y and Feng D L 2010 *Phys. Rev. B* **81** 014526

[21] Marzari N and Vanderbilt D 1997 *Phys. Rev. B* **56** 12847

[22] Souza I, Marzari N and Vanderbilt D 2001 *Phys. Rev. B* **65** 035109

[23] Kuroki K, Onari S, Arita R, Usui H, Tanaka Y, Kontani H and Aoki H 2008 *Phys. Rev. Lett.* **101** 087004

[24] Böhm T, Kretzschmar F, Baum A, Rehm M, Jost D, Ahangharnejhad R H, Thomale R, Platt C, Maier T A, Hanke W, Moritz B, Devereaux T P, Scalapino D J, Maiti S, Hirschfeld P J, Adelmann P, Wolf T, Wen H H and Hackl R 2015 arXiv: 1703, 07749 [cond-mat.supr-con]

[25] Wang W S, Xiang Y Y, Wang Q H, Wang F, Yang F and Lee D H 2012 *Phys. Rev. B* **85** 035414

[26] Xiang Y Y, Wang W S, Wang Q H and Lee D H 2012 *Phys. Rev. B* **86** 024523

[27] Xiang Y Y, Wang F, Wang D, Wang Q H and Lee D H 2012 *Phys. Rev. B* **86** 134508

[28] Wang W S, Li Z Z, Xiang Y Y and Wang Q H 2013 *Phys. Rev. B* **87** 115135

[29] Xiang Y Y, Yang Y, Wang W S, Li Z Z and Wang Q H 2013 *Phys. Rev. B* **88** 104516

[30] Yang Y, Wang W S, Xiang Y Y, Li Z Z and Wang Q H 2013 *Phys. Rev. B* **88** 094519

[31] Wang Q H, Platt C, Yang Y, Honerkamp C, Zhang F C, Hanke W, Rice T M and Thomale R 2013 *Europhys. Lett.* **104** 17013

[32] Yang Y, Wang W S, Liu J G, et al. 2014 *Phys. Rev. B* **89** 094518

[33] Wang W S, Yang Y and Wang Q H 2014 *Phys. Rev. B* **90** 094514

[34] Christianson A D, et al. 2008 *Nature* **456** 930

[35] Lumsden M D, Christianson A D, Parshall D, Stone M B, Nagler S E, MacDougall G J, Mook H A, Lokshin K, Egami T, Abernathy D L, Goremychkin E A, Osborn R, McGuire M A, Sefat A S, Jin R, Sales B C and Mandrus D 2009 *Phys. Rev. Lett.* **102** 107005

[36] Qiu Y, Bao W, Zhao Y, Broholm C, Stanev V, Tesanovic Z, Gasparovic Y C, Chang S, Hu J, Qian B, Fang M and Mao Z 2009 *Phys. Rev. Lett.* **103** 067008

[37] Babkevich P, Roessli B, Gvasaliya S N, Regnault L P, Freeman P G, Pomjakushina E, Conder K and Boothroyd A T 2011 *Phys. Rev. B* **83** 180506

[38] Dai P 2015 *Rev. Mod. Phys.* **87** 855

[39] Kuhn S J, Kidder M K, Parker D S, Cruz C dela, McGuire M A, Chance W M, Li L, Debeer-Schmitt L, Ermentrout J, Littrell K C, Eskildsen M R and Sefat A S 2017 *Physica C* **534** 29